Sensors and Actuators B 137 (2009) 617–629

Contents lists available at ScienceDirect

Sensors and Actuators B: Chemical

journal homepage: www.elsevier.com/locate/snb

Designing and optimizing microsensor arrays for recognizing chemical hazards in complex environments☆

Baranidharan Raman[a,b], Douglas C. Meier[a], Jon K. Evju[a], Steve Semancik[a,*]

[a] Chemical Science and Technology Laboratory, National Institute of Standards and Technology (NIST), 100 Bureau Drive MS8362, Gaithersburg, MD 20899-8362, USA
[b] Laboratory of Cellular and Synaptic Neurophysiology, National Institute of Health (NICHD, NIH), 35 Convent Drive Room 3A106, MSC 3715, Bethesda, MD 20892-3715, USA

ARTICLE INFO

Article history:
Received 2 October 2008
Received in revised form
25 November 2008
Accepted 30 November 2008
Available online 25 December 2008

Keywords:
Microsensor arrays
Metal oxide sensors
Toxic industrial chemicals
Statistical analysis
Material evaluation
Selection and optimization

ABSTRACT

A generic approach to designing microsensor arrays for complex chemical sensing tasks is described and demonstrated for the problem of recognizing chemical hazards at sublethal concentrations, under varying ambient conditions, and in the presence of interfering chemicals. We present statistical methods to systematically assess the analytical information obtained from the conductometric responses of chemiresistive elements at different operating temperatures, test their reproducibility, and determine an optimal set of material compositions to be incorporated within an array for individual species recognition. These advances are critical to the production of pre-programmed microsensors for non-invasive trace analyte detection relevant to homeland security, medical diagnostics, and other applications.

1. Introduction

Detection of trace quantities of toxic industrial chemicals (TICs), an application of critical importance for homeland security, poses a unique set of analytical challenges. While heightened sensitivity to a spectrum of chemical hazards is necessary for detection of TICs at relevant concentrations, substantial selectivity is necessary to rapidly extract the pertinent information about the presence (or absence) of a chemical hazard under myriad possible background conditions defined by ambient temperature, humidity, and the presence of common interfering chemicals. The chemically aggressive nature of TICs and some interfering gases also enforce other demands, such as robustness for reliable recognition of the targets for extended time periods. In addition to the analytical complexity of the problem, instrument and sensor developers are typically also bound by stringent constraints on response times, instrument size, power consumption, signal reproducibility, and cost, in order to achieve early warning capabilities and facilitate affordable wide-networked deployment. Current approaches to detection of chemical hazards include the use of a variety of instruments and sensing technologies: spectrometric approaches (gas chromatography [1], mass spectroscopy [2], ion-mobility spectroscopy [3], and their combinations [4–6]), piezoelectric devices [7,8], optical techniques [9,10], electrochemical devices [11,12] and chemiresistors [13–15]. In this work, we present a novel approach to this problem involving chemiresistive microsensor arrays with fine temperature control.

To simulate a problem that sufficiently captures these issues, we examined a target matrix that features five high-priority chemical hazards: ammonia (NH), hydrogen cyanide (HCN), chlorine (CL), ethylene oxide (EO), and cyanogen chloride (CK). NH and EO are common TICs that are also employed as precursors in the manufacture of explosives, narcotics, and polymers. Beyond their industrial uses, HCN and CK are blood agents and CL is a pulmonary agent that inhibits the ability to breathe [16,17]. The concentrations of these chemicals that pose an immediate danger to life and health (IDLH) are given in Fig. 1A. To approximate relevant real-world conditions, each of these five chemical hazards at their IDLH concentrations was introduced individually into synthetic air containing three different relative humidities (10, 30 or 70%) or infused with the vapors of any one of the following common products: bleach (Clorox [18]), interior house paint, window cleaner (Windex [18]) and floor stripper (ZEP [18]) (see Fig. 1B). The last three target presentations were graded such that the concentration gradually increased in fixed steps until it reached the IDLH concentration and was removed in a similar gradual fashion.

☆ Elements of this paper presented at the International Meeting on Chemical Sensors 2008 (IMCS-12), July 13–16, 2008, Columbus, OH, USA.

* Corresponding author. Tel.: +1 301 975 2606; fax: +1 301 975 2643.
E-mail address: steves@nist.gov (S. Semancik).

0925-4005/$ – see front matter © 2008 Elsevier B.V. All rights reserved.
doi:10.1016/j.snb.2008.11.053

(A)

Calibrated analytes	Chemical Formula	Abbreviations used	Vapor pressure (20 °C)	IDLH concentrations
Ammonia	NH_3	NH	891 k Pa	300 μmol/mol
Hydrogen cyanide	HCN	HCN	82.3 k Pa	50 μmol/mol
Chlorine	Cl_2	CL	638 k Pa	10 μmol/mol
Cyanogen chloride	CNCl	CK	133 k Pa	20 μmol/mol
Ethylene oxide	C_2H_4O	EO	146 k Pa	800μmol/mol

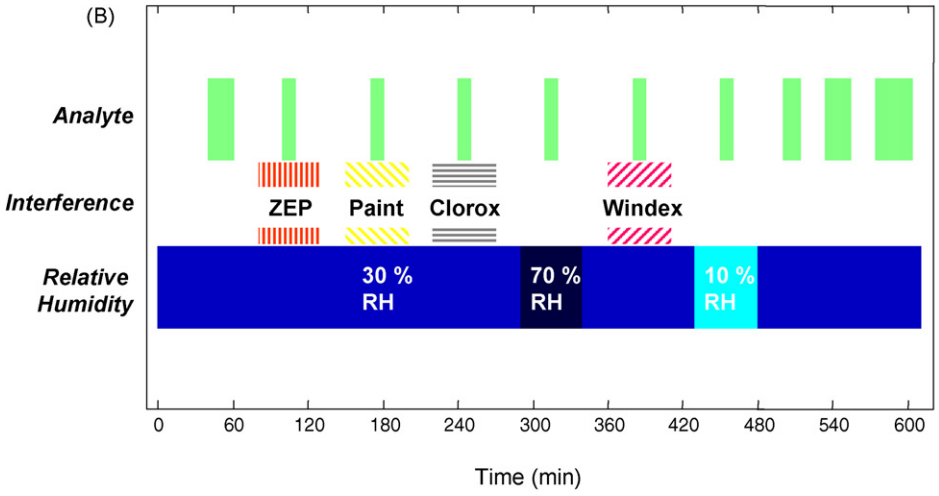

Fig. 1. Chemical hazards, interferences, and humidity levels constituting the test matrix of the present study. (A) Five toxic industrial chemicals (TICs), their vapor pressures at 20 °C, and their immediate danger to life and health (IDLH) concentration levels. (B) Analyte delivery protocol used for data collection. The blue bar (bottom row) indicates the humidity level at different time periods within a cycle. Three different humidity levels were used in this study: 10% RH, 30% RH and 70% RH. Four common, commercially available interferences (middle row): bleach (Clorox [18]), latex interior house paint, window cleaner (Windex [18]) and floor stripper (ZEP [18]), each at 1% of their saturated vapor concentration, were used to simulate realistic scenarios. The color-coded bars indicate the delivery periods of each of these interferences during a cycle. The green bars (top row) mark the periods during which any one of the five TICs is introduced. The last three target analyte introductions were graded such that the concentrations gradually change from zero to maximum and then return to baseline in a similar fashion. Two back-to-back cycles, each lasting ~10 h, constitute a training run. This protocol was repeated for each of the five TICs. (For interpretation of the references to color in this figure legend, the reader is referred to the web version of the article.)

This detector evaluation study consisting of 42 different target-background combinations presents a recognition problem of considerable analytical complexity. A critical step in designing an array-based solution to deal with this sensing task concerns the evaluation and selection of sensing materials. In this paper, we present a novel statistical approach to address this important issue. We show how a metric based on correlation between sensor responses can be used to assess their similarity/orthogonality, test their reproducibility, and understand the basis of distinguishable chemical signatures. Furthermore, we present qualitative and quantitative approaches to determine the sufficiency of the chosen materials for sensing targets in the test matrix and determine an optimal array configuration for the desired application.

2. Experimental

2.1. Microhotplate platforms

A suitable platform that provides considerable benefits in meeting many of the stated analytical requirements is the MEMS-based microhotplate array [19]. Each array element (Fig. 2A) contains three functional components (see layered schematic in Fig. 2B): a polycrystalline silicon resistor for heating, a chemically sensitive film, and interdigitated platinum electrodes that enable measurement of the conductance of the sensing film that is deposited onto the array element. This miniaturized device (≈100 μm, with a mass ≈250 ng) has a thermal time constant of a few milliseconds, and an operating temperature range from ambient to 500 °C. The localized temperature control offered by microhotplates, along with their fast heating/cooling characteristics, makes them ideal both for self-lithographic, thermally activated chemical vapor deposition (CVD) processes [20] and for device operation with temperature programming, wherein each element is independently cycled through multiple temperatures during sensor measurements. Each microsensor array consists of a collection of such individually addressable, temperature-controlled elements as shown in Fig. 2C. A 40-pin dual in-line packaged device is shown in Fig. 2D.

2.2. Sensing materials

For the purposes of broad-spectrum detection required by this task, we employed the following four semiconducting metal oxide films: tin (IV) oxide (SnO_2), tin (IV) oxide coated with titanium (IV) oxide (SnO_2/TiO_2), titanium (IV) oxide (TiO_2), and titanium (IV) oxide coated with ruthenium oxide (TiO_2/RuO_x). Metal oxide semiconductor films were chosen as the chemically sensitive component in these devices for a variety of reasons. They are known to undergo chemical interactions with gas species ranging from surface-mediated oxidation of analyte gases to charge transfer upon analyte chemisorption [21–23]. These interactions, as a result of electron transfers between adsorbed gases and a surface depletion layer, cause a repeatable change in the electrical conductance of the film, thus yielding a measurable and recognizable signal [24]. These conductance changes have been shown to be temperature

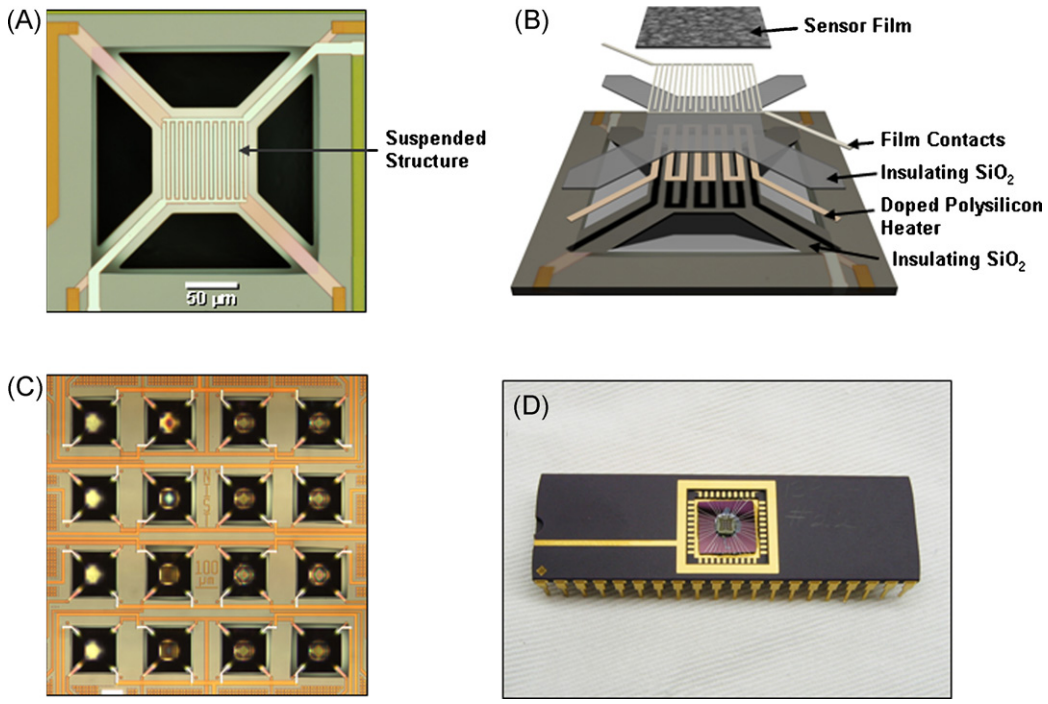

Fig. 2. Microsensor array platforms. (A) An optical microscopy image of a single microhotplate microsensor element. (B) A layered schematic showing the three primary components of the microsensor elements: polycrystalline silicon heater, interdigitated platinum electrodes, and metal oxide sensing film. (C) A microsensor array with 16 individually addressable, temperature-controlled elements. (D) A 40-pin dual in-line packaged microsensor device.

dependent, materials dependent, and most importantly, analyte dependent for compounds from the simple (e.g., CO) to the complex (e.g., chemical warfare agent molecules) [15,24,25]. The oxides are also robust materials capable of withstanding wide excursions of temperature we use to enhance the analytical content of the signal stream.

Each of the chosen films was deposited onto the array using CVD processes (see below). Fig. 3A shows the optical images of these different films, and the sensing film microstructures are shown in Fig. 3B. The metal oxide sensing films themselves, while robust, are only partially selective and will respond to many analytes. However, it can be expected that any given analyte/sensing material pair will generate distinguishing characteristics in its electrical conductance profile due to temperature-dependent variations in chemical interactions at the surface. Hence, each sensing film is programmed to cycle through many temperatures in a pulsed mode such as that illustrated in Fig. 4, in order to capture a greater range of temperature-dependent interactions between analytes and sensing films. This mode of operation, which is expected to greatly enhance the analytical content of the microsensor signal over that of fixed-temperature sensing, is referred to as temperature-programmed sensing (TPS) [15].

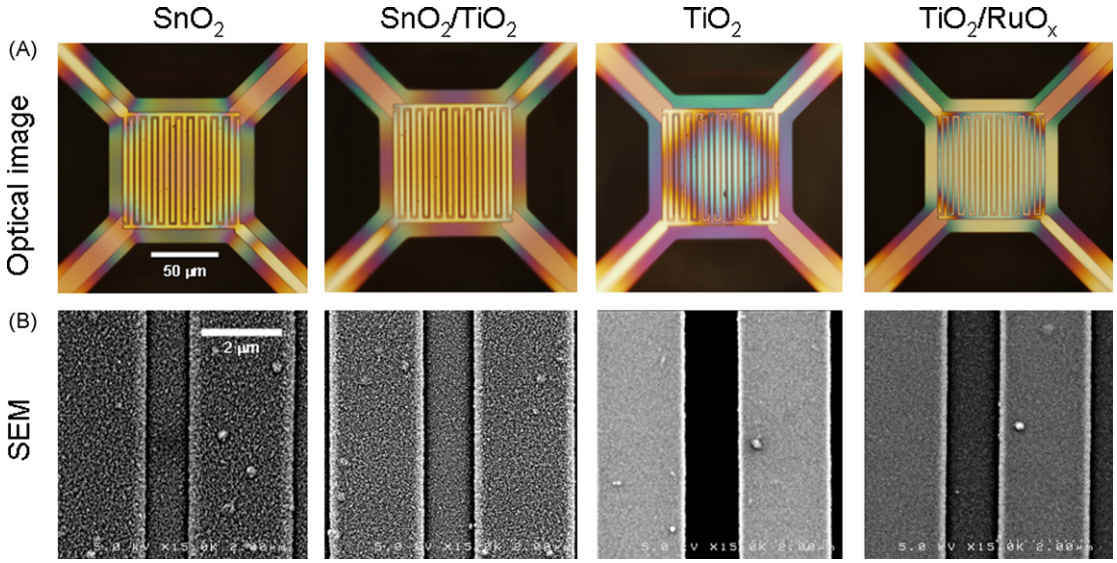

Fig. 3. Controlling material composition to impart selectivity. (A) Optical microscopy images of the four films used in this study (size of scale bar applies to all panels): tin oxide (SnO_2), tin oxide coated with titanium oxide (SnO_2/TiO_2), titanium oxide (TiO_2) and titanium oxide coated with ruthenium oxide (TiO_2/RuO_x). Four copies of each material were used in arrays for this work. (B) Scanning electron microscopy images of the four films (size of scale bar applies to all panels).

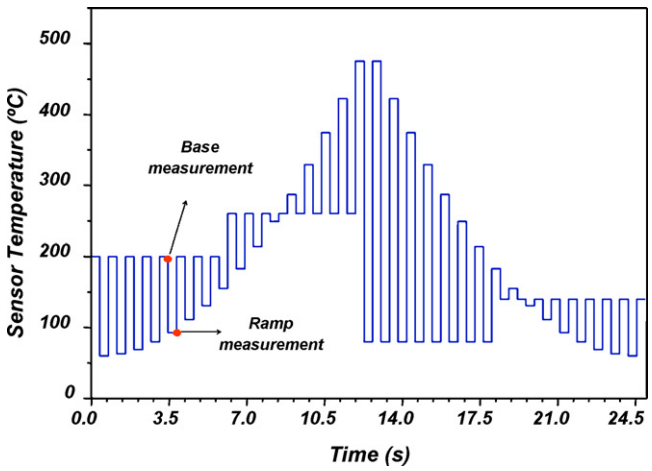

Fig. 4. Temperature programmed sensing. The temperature program used to operate the sensing elements toggles the temperature between 32 ramp values that sample most of the temperature range of the device and four different baseline temperature values to allow "relaxation" toward some initial state prior to each ramp temperature. Moreover, different baselines also allow different film–analyte interactions (adsorption/desorption, decomposition, and reaction) at the sensing surface prior to the ramp measurements. The dwell time at each temperature (period of the pulse) was typically on the order of 200 ms. A conductance measurement was made at each base and ramp temperature, but only the ramp values were used for further analysis in this study.

2.3. Sensor fabrication

Thin metal oxide sensing films were fabricated using a thermally activated single-source CVD process described below. The precursors used to deposit sensing films were delivered from temperature-controlled vessels under flow of Ar delivered at 7 standard cm^3/min (sccm). All bypass lines of precursors not in use were also maintained at 7 sccm Ar flow in order to prevent back-flow contamination of other precursors and their delivery lines. The approximate space velocity at the sensor surface is 17,000 cm/min. All precursor delivery lines were maintained at 55 °C; the precursor sources were temperature controlled as follows: tin(IV) nitrate anhydrous at 30 °C, titanium(IV) 2-propoxide at 30 °C, and triruthenium dodecacarbonyl at 65 °C. The pressure in the CVD chamber was maintained at ≈3 Pa by an oil-free vacuum pump. Each precursor was given a 10-min chamber equilibration period prior to film deposition. Furthermore, after a deposition cycle was completed, clean Ar was delivered through all delivery lines for 10 min prior to starting the next precursor, in an effort to reduce cross-contamination. After the initial equilibration period, the target microhotplate element(s) were heated to 375 °C, decomposing the precursor to form localized thin solid film(s). The deposition period for the SnO_2 and TiO_2 pure films was 20 and 120 s, respectively. For the mixed metal oxide films, the two materials were deposited in series: SnO_2 for 5 s followed by TiO_2 for 60 s and TiO_2 for 60 s followed by Ru for 90 s. The deposited films were subsequently removed from vacuum, placed in a test system flowing zero-grade dry air at 1 standard l/min (slm), corresponding to a space velocity of roughly 600 cm/min, and gradually (≈14 °C/min) elevated to 400 °C, where they were annealed for 30 min.

2.4. Analyte delivery

A custom gas delivery manifold was used to separately deliver four analyte stream components: target-laden zero-grade dry air, interference-laden dry air, humid air, and balance dry air. The manifold features non-reactive tubing for each input stream connected to a central cell, where sample blending occurred. Metered concentrations of analytes were delivered either from pre-blended commercial cylinders (for more stable compounds exhibiting higher vapor pressures, such as HCN and NH) or from analyte generators loaded with calibrated permeation vessels (for more reactive, low vapor pressure species, such as CK and EO). Interference vapors were introduced by bubbling metered quantities of dry air through vessels containing the interference candidate, after which the saturated gas stream was delivered via dedicated lines to the central cell (thus interferences are reported in percent saturation). In order to reduce biases stemming from fractional evaporation of interference mixtures, the liquid sources were replaced regularly. Interference introduction was performed using this method for final concentrations of up to 1% saturation at room temperature. According to their MSDS, the vapor pressures of the interferences are all roughly equal to that of water, about 2800 Pa at 23 °C [26]. Thus the molar concentrations of the generated interferences are roughly 280 μmol/mol, a value approximating that of each analyte studied. Humid air was generated by metering zero-grade dry air through a dew point generator. Test cell humidity could thus be varied between 0% relative humidity (RH) and 90% RH at 25 °C using this apparatus. The water vapor concentrations at 10% RH, 30% RH, and 70% RH were 2.8, 8.4, and 19.6 mmol/mol, respectively. The balance dry air was adjusted such that at any point in time, the sum total flow rate of these four "single-component" streams into the central cell was 1 slm. A sensor cell that housed the microsensor array was placed downstream from the mixing manifold.

2.5. Data analysis

All analyses were done using custom programs in MATLAB [18]. Conductance measurements of each element for the complete cycle of 32 ramp temperatures (see Fig. 4) were concatenated to form a multi-dimensional sensor response that was used in all analyses.

To analyze the similarity/orthogonality of responses of any two materials (M_1, M_2) at two operating temperatures (T_1, T_2), we used Pearson's correlation coefficients. If $g(M_1, T_1)$ is a one-dimensional vector of conductance measurements made at each of the different training conditions (see Fig. 1B) using a material M_1 at temperature T_1, and $g(M_2, T_2)$ a one-dimensional vector of conductance measurements made using sensing material M_2 at temperature T_2, then the correlation between responses of M_1 at T_1 and M_2 at T_2 is calculated as

$$\frac{n\sum g(M_1,T_1)g(M_2,T_2) - \sum g(M_1,T_1)\sum g(M_2,T_2)}{\left(\left(n\sum g(M_1,T_1)^2 - \left(\sum g(M_1,T_1)\right)^2\right) \times \left(n\sum g(M_2,T_2)^2 - \left(\sum g(M_2,T_2)\right)^2\right)\right)^{1/2}} \quad (1)$$

where n in the number of collected samples, and $g(M_1, T_1)$ is the measured conductance from material M_1 at temperature T_1. An illustration of correlation analysis between SnO_2 isotherms at 60 and 480 °C is shown in Fig. 5. Only the absolute values of the correlation coefficients with significance $P < 0.001$ are shown in Figs. 5–10. For visualizing the sensor response, we used linear discriminant analysis (LDA) [27], which finds directions that maximize separation between classes and minimize variance within a single class; i.e. eigenvectors of $S_W^{-1}S_B$ where S_W and S_B are within and between class covariance matrices (see below). In this work, we have used LDA to determine what information comes from which films and whether the chosen film composition and temperature programs have sufficient information for identifying all five TICs in different background conditions.

To optimize the array configuration, we define the following objective function with three components:

$$O = \underbrace{\gamma_1 J}_{\text{Maximization term}} - \underbrace{\gamma_2 N_1}_{\text{Penalty term for materials}} - \underbrace{\gamma_3 N_2}_{\text{Penalty term for array size}} \quad (2)$$

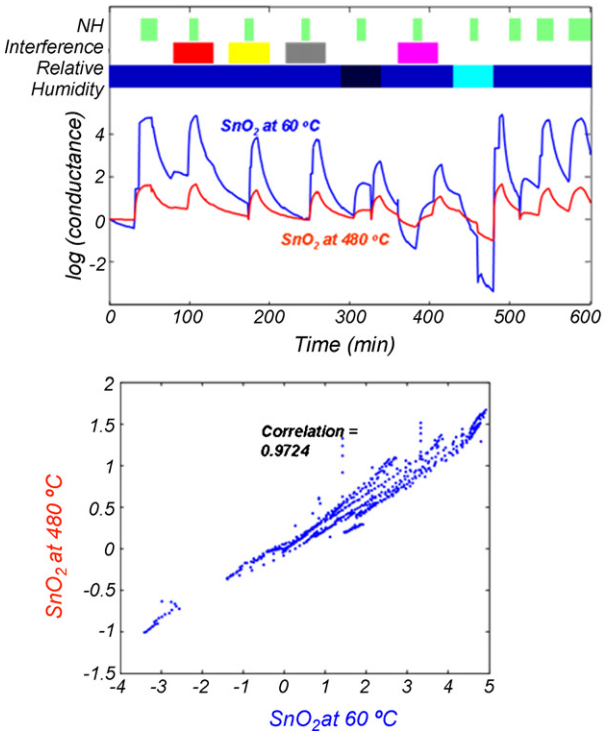

Fig. 5. Illustration of correlation analysis. (A) SnO_2 electrical conductance isotherms at 60 °C (blue) and 480 °C (red) in response to different conditions indicated schematically at the top of the figure (refer to Fig. 1B). (B) The responses at 60 °C vs. 480 °C to different conditions lie along the diagonal showing a greater degree of correlation between the two isotherms. (For interpretation of the references to color in this figure legend, the reader is referred to the web version of the article.)

where J is the maximization term that takes into account the sufficiency of solution; i.e., separability of the five TIC clusters from different background conditions and from each other, N_1 and N_2 are the number of different materials used and the array size respectively, and γ_1, γ_2, γ_3, are component weights. The two penalty terms allow comparison between solutions with different numbers of materials and array sizes. To increase the objective function, each new material or array element must increase the TICs cluster separability sufficiently to compensate for its cost.

The measure of cluster separability derived from Fisher's LDA [27] can be defined as follows:

$$J = \frac{trace(S_B)}{trace(S_B) + trace(S_W)} \tag{3}$$

where S_W and S_B are the within-cluster and between-cluster scatter matrices, respectively, defined as follows:

$$S_W = \sum_{q=1}^{Q} \sum_{x \in \omega_q} (x - \mu_q)(x - \mu_q)^T \tag{4}$$

$$S_B = \sum_{q=1}^{Q} (\mu_q - \mu)(\mu_q - \mu)^T \tag{5}$$

$$\mu_q = \frac{1}{n_q} \sum_{x \in \omega_q} x \quad \text{and} \quad \mu = \frac{1}{n} \sum_{\forall x} x \tag{6}$$

where x is a linear projection of sensor response along $Q-1$ linear discriminant axes, Q is the number of conditions (six clusters corresponding to the following conditions: NH, HCN, CL, EO, CK and all background conditions collectively), μ_q and n_q are the mean vector and number of examples for condition q, respectively, n is the total number of examples in the dataset, and μ is the mean vector of the entire distribution. Being the ratio of the spread between classes relative to the spread within each class, the measure J increases monotonically as classes become increasingly more separable.

Classification analysis was done using the non-parametric, local k-nearest neighbor scheme ($k=3$) with leave-one-out cross-validation. A Euclidean distance metric was used to find the nearest neighbors in the multi-dimensional sensor conductance response space.

3. Results

3.1. Assessment of similarity and reproducibility of materials

To assess similarity/orthogonality of conductometric responses generated by sensor materials and temperature programs, we use a measure based upon pair-wise correlation. For simplicity, we focus our discussion on the problem of NH detection in the presence of each of the four interferences and at three different humidity conditions (parallel results for the other four TICs are presented in Fig. 8). The data discussed in these analyses were generated in a series of "training runs" wherein the sensor arrays were exposed to the analyte stream as summarized in Fig. 1B. This training data not only aids in materials response and temperature program assessment, but also serves as the reference database by which subsequent alarm decisions can be made.

3.1.1. Is different information really acquired at different temperatures?

In order to determine whether the TPS mode of operation generates additional information from each film composition, we compute, for each film type, the correlation between its responses to different conditions at different temperatures. Fig. 5 shows an example of this correlation analysis between SnO_2 responses at 60 and 480 °C (isotherms). A more detailed plot illustrating the correlation coefficients for the four films for the NH detection problem is shown in Fig. 6. Each pixel shows the correlation between two isotherms of the same material. Only the absolute values of the significant correlations ($P<0.001$) are shown (the t-test is not valid for the diagonal elements, which represent self-correlations, as the denominator becomes zero). Lighter pixels indicate higher correlations and darker pixels represent lower correlations. The greater the correlation, the more similar or redundant is the information generated.

The correlation plots shown in Fig. 6 reveal that in the case of the TiO_2 films with and without RuO_x coating, the lower temperature responses correlate well amongst themselves, but not with those obtained at higher temperatures. Similarly, the high temperature responses correlate well only amongst themselves. This lack of correlation between the two temperature bands indicates that different analytical information is obtained from these bands. Interestingly, the TiO_2/RuO_x film shows a lack of correlation between the low-temperature features on the upward vs. downward portion of the temperature program, indicating a dependence on thermal history. In the case of SnO_2 films both with and without TiO_2, all temperature features appear to be well-correlated (notice the change in the scale bar). However, as in the case of TiO_2 films, the high temperature features and low-temperature features show a greater degree of correlation only amongst themselves. Hence, for the four sensing materials, different information is generated at low and high temperatures.

3.1.2. Is different information generated by different film types?

The self-correlations computed between temperature features within film types do not provide any insights into the similarity/orthogonality across multiple materials. To evaluate this, we compute cross-correlation across isotherms of different film types.

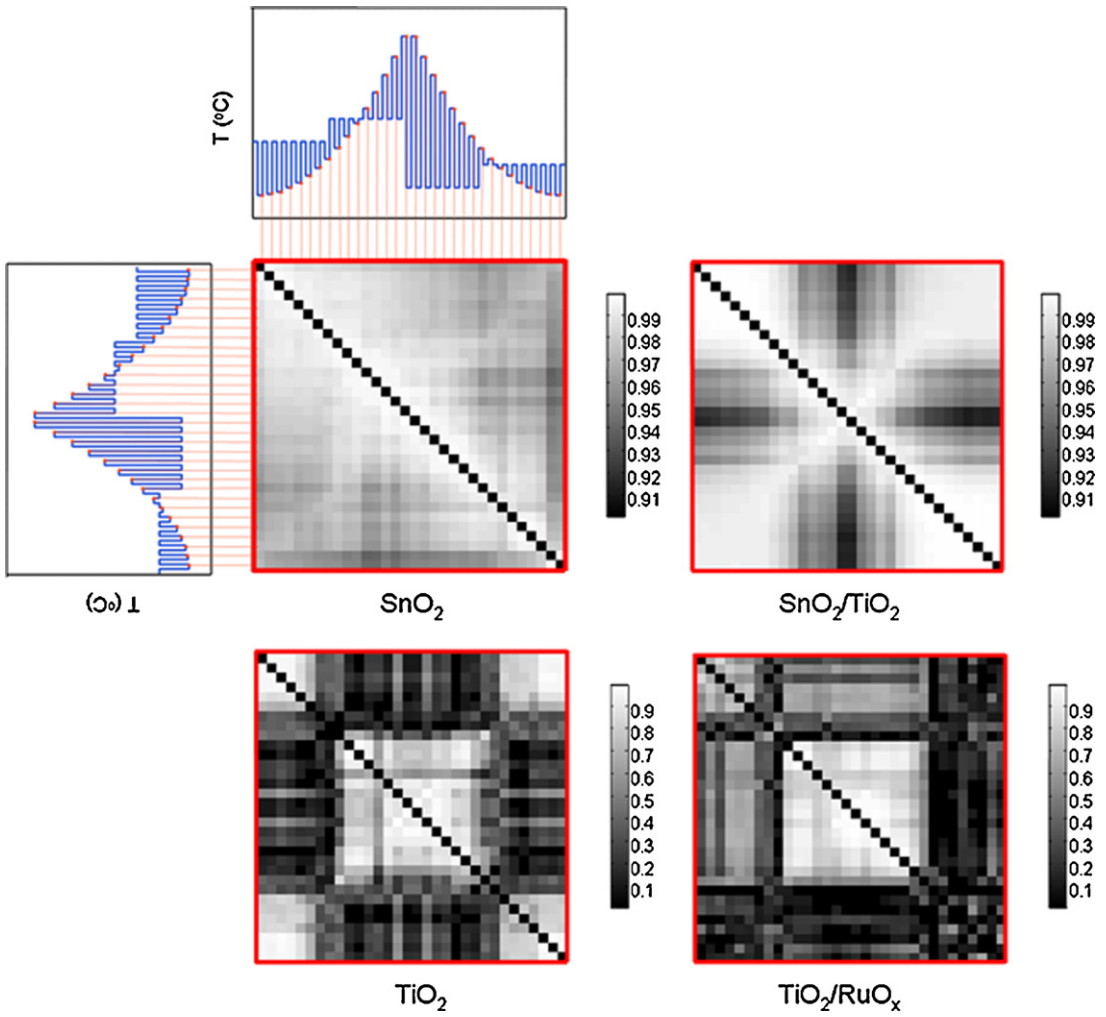

Fig. 6. Correlation analysis to assess similarity/orthogonality of material-temperature combinations. Color-coded representation of the correlation coefficients between conductometric responses of each of the four sensing materials at different temperatures. Note that light areas indicate high correlation and dark areas show lower degrees of correlation. Only the absolute values of correlations that are significant ($P < 0.001$) are shown.

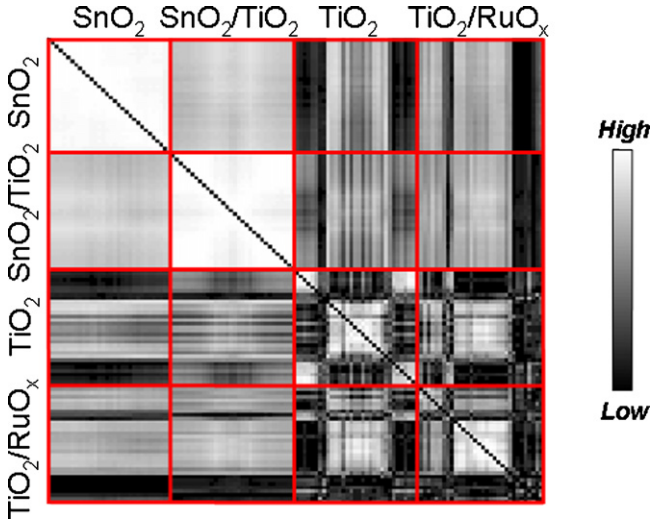

Fig. 7. Cross-correlation analysis. Lower correlation between responses of different film types at different temperatures reveal that the chosen sensing materials contribute non-redundant information for recognizing NH.

Fig. 7 shows the cross-correlation plots for a single copy of the four different metal oxides. The diagonal blocks show self-correlations and are essentially the same as in Fig. 6. We observe lower correlations between different film types, indicating that the four materials contribute non-redundant information towards NH recognition. Parallel results on the other four analytes are presented in Fig. 10. Note that the correlation patterns change as a function of analyte identity.

3.1.3. *Reproducibility of the sensing films*

To determine response reproducibility of the chosen films, we made four replicas of each film type in a 16-element microsensor array. Fig. 9 shows cross-correlation across two copies of each material. A qualitative evaluation of the reproducibility of the sensing materials can be made by visually comparing the correlation patterns. Copies of a single film type (e.g. SnO_2 vs. SnO_2) show similar correlation patterns across temperature features, indicating that the films produced through the CVD process generate information that is highly reproducible between devices of equivalent manufacture. However, amongst the four film types used, the TiO_2/RuO_x films show the least-conserved cross-correlation patterns, especially at lower temperatures, indicating lower repro-

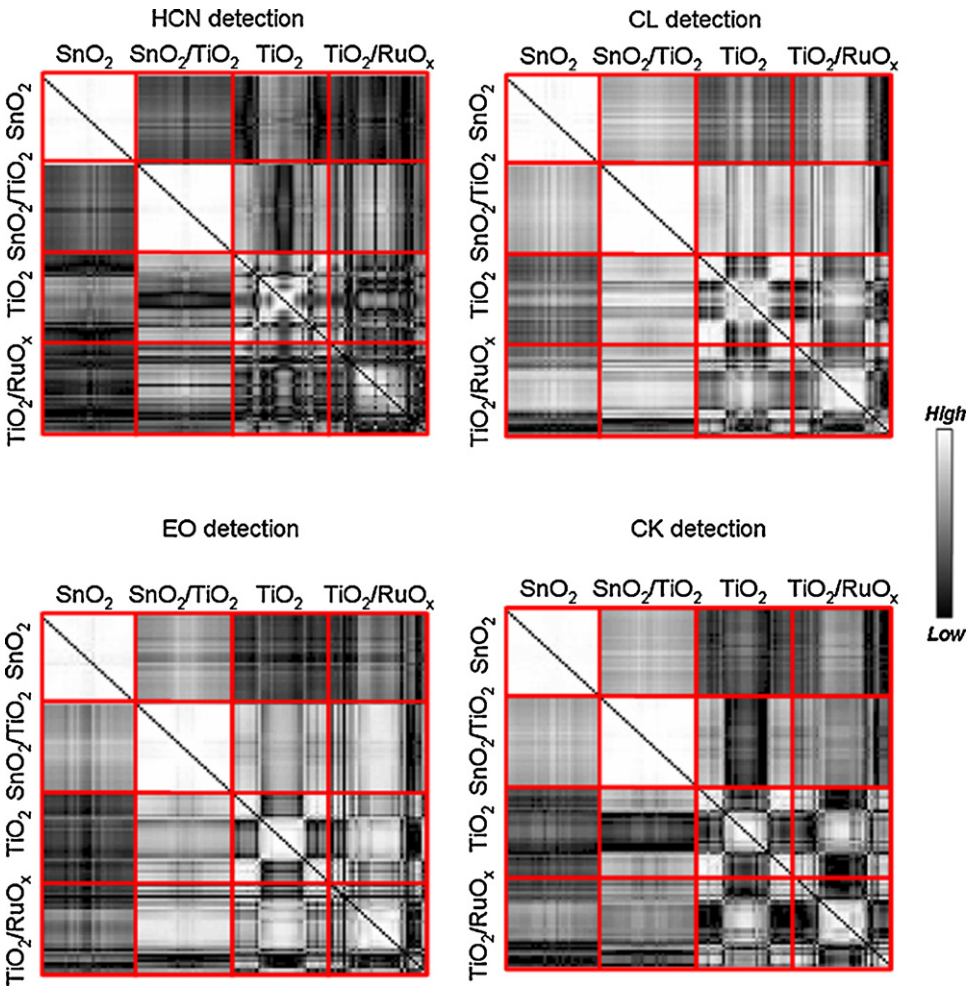

Fig. 8. Basis of distinguishable chemical signatures. Cross-correlation patterns between different film types are unique for each TIC identification problem: (A) HCN recognition, (B) CL recognition, (C) EO recognition, and (D) CK recognition.

ducibility compared to the other three film types used in these studies. A quantitative evaluation of reproducibility based on the correlation coefficients from four copies of each material is presented in Fig. 10.

3.2. Dimensionality reduction analysis

The correlation analysis uncovers relationships between conductometric responses of different materials at different operating temperatures, but does not provide insights about what information is contributed by each film type and whether the chosen materials and temperature programs provide sufficient analytical information to allow species recognition. In order to determine this, we visualize the multi-dimensional sensor array response using linear discriminant analysis [27]. Fig. 11 shows the scatter plot of the multi-dimensional sensor response obtained by concatenating the sensor conductance values at the 32 ramp temperatures of a single sensing film (SnO_2 at 32 temperatures or SnO_2/TiO_2 at 32 temperatures or TiO_2 at 32 temperatures or TiO_2/RuO_x at 32 temperatures) and projecting it onto the first three linear discriminant axes. Each three-dimensional color-coded sphere indicates one of the six possible conditions of interest: presence of NH (red), HCN (magenta), CL (yellow), EO (cyan), CK (black), and any of the tested backgrounds without hazards (blue). Each condition in turn could belong to any one of the several sub-conditions shown in Fig. 1B; for example, red samples include all sensor responses to NH, with or without the four different interferences and at all three humidity conditions. From the LDA plots it is clear that none of the film types alone can provide enough analytical information for the recognition of all five TICs in different background conditions. However, when information from two copies of each film type is combined (8 films × 32 tempera-

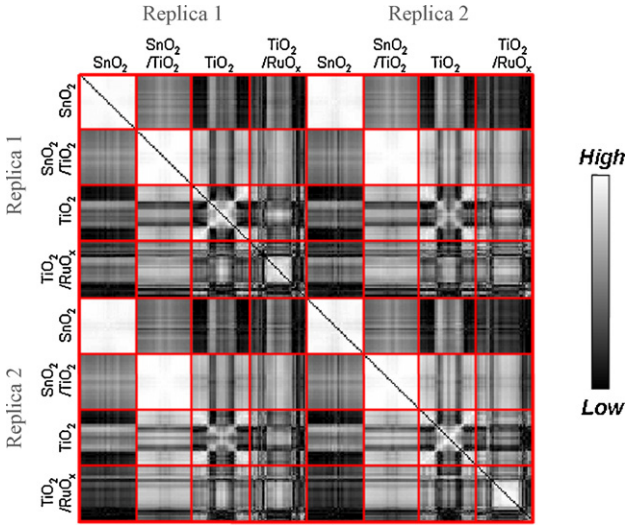

Fig. 9. Reproducibility analysis. Correlations across two copies of each sensing material deposited onto a 16-element array for the NH detection problem.

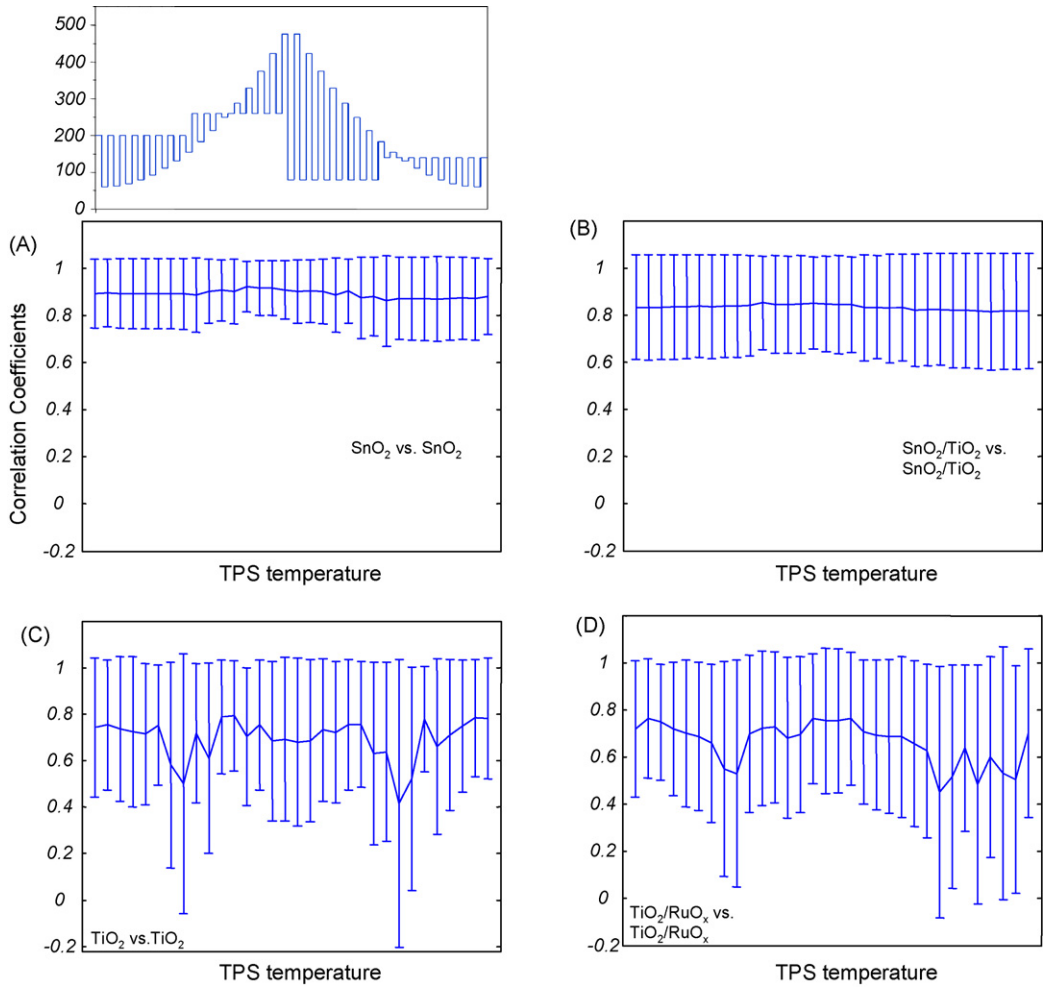

Fig. 10. Quantitative summary of reproducibility analysis. Self-correlations for each of the film types at different temperatures are shown. The higher the correlations coefficients are, the better the response reproducibility is.

tures = 256-dimensional feature vector), as shown in Fig. 12, all of the five chemical hazards can be detected and discriminated.

3.3. Array optimization

To determine the optimal material composition for a given sensing problem, we define an objective function that takes into account the sufficiency of a solution (i.e. TICs cluster separability), and a penalty term for additional resources used, e.g. number of different materials used, or the size of an array (refer to Eq. (2) in Section 2 for details). We use this method to optimize the array configuration for detection and discrimination of multiple targets in different background conditions defined in Fig. 1B.

The ability to distinguish TIC clusters from each other and from the background improves (refer to Eq. (3) in Section 2 for a qualitative definition) as we incorporate redundancy (see Fig. 13) or diversity (see Fig. 14) into the array. Even though copies of SnO_2 provided highly correlated information, redundancy helped lower the detection threshold of the array by averaging out uncorrelated noise across multiple copies. For example, HCN, EO and CK, which cannot be detected using a single SnO_2 sensor alone, can be recognized with four copies of SnO_2 (see LDA cluster plots in Fig. 13). This form of sensitivity enhancement, where the detection limit for the collection of like elements is lower than any of its individual elements is generally referred to as hyperacuity [28]. Increasing diversity, on the other hand, added orthogonal information about different hazards and thereby improved the cluster separability.

Fig. 15(A) compares the different configurations of an 8-element array for this problem. The best solution, in this case, is obtained with four copies each of the SnO_2 and SnO_2/TiO_2 films. A qualitative

Table 1
Classification performance with leave-one-out cross-validation.

Delivered	Detected					
	Background (%)	NH (%)	HCN (%)	CL (%)	EO (%)	CK (%)
Background (%)	97.13	0.0065	0.0056	0.0084	0.0041	0.0041
NH (%)	0.0813	91.87	0	0	0	0
HCN (%)	0.1063	0	89.38	0	0	0
CL (%)	0.2366	0	0	76.34	0	0
EO (%)	0.1402	0	0	0	85.98	0
CK (%)	0.2977	0	0	0	0	70.23

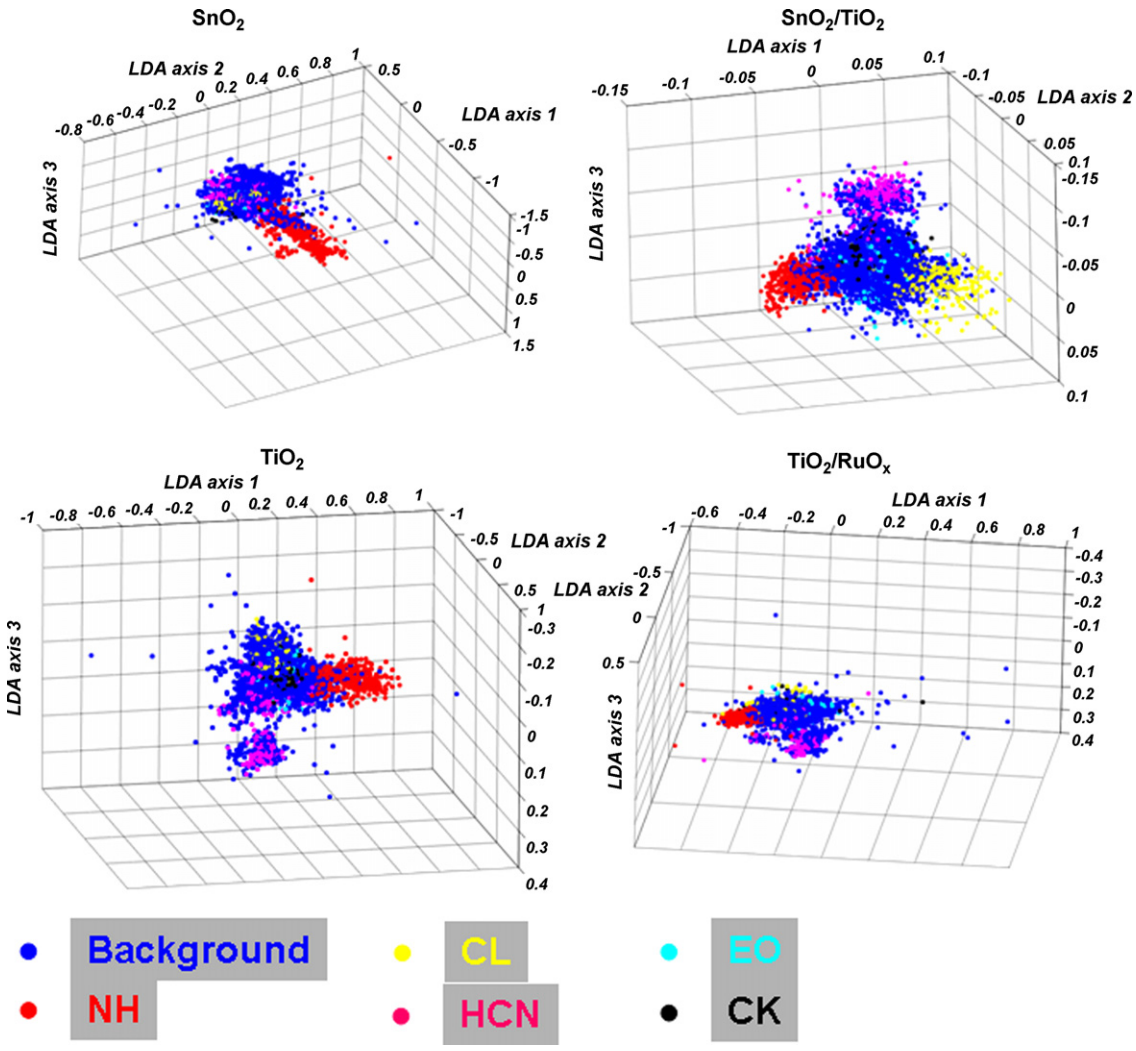

Fig. 11. Dimensionality reduction analysis. Scatter plots of the conductometric responses of different film types at different conditions (see Fig. 1B) after dimensionality reduction using Fisher's linear discriminants.

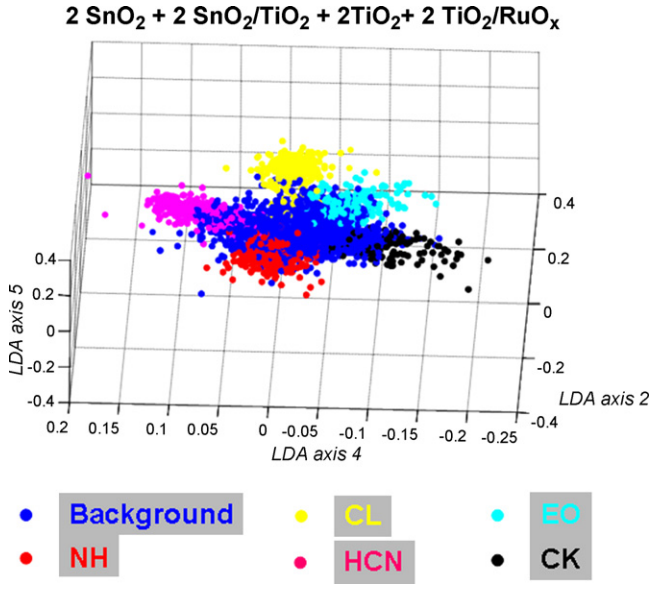

Fig. 12. Qualitative determination of sufficiency of analytical information. LDA scatter plots when information from two copies of the four materials, each operated using the temperature program shown in Fig. 4, are used to identify the five TICs.

determination of the sufficiency of this optimized array configuration is provided in Fig. 15 (B). A detailed quantitative summary of the classification performance for data collected over a period of several weeks, including repeats of each experimental condition, is presented in Table 1 to validate the short-term durability of our approach. We note that all of the TIC introductions were correctly recognized albeit with some lag at the analyte onset and offset. Most sensor evaluation studies [14,29,30] to date limit response analysis to only steady-state measurements. The goal of our work, however, was to provide a more stringent performance evaluation in order to achieve near-real-time target detection for field deployment of the devices. Hence, no manual interventions were allowed to select baselines [13,14,29,30] and determine whether steady-state had been reached.

4. Discussion

We have presented a modular approach for designing an array-based solution, using microhotplate platforms with metal oxide chemiresistors, for recognizing five different TICs in complex backgrounds. Semiconducting metal oxides were shown to be effective for the purposes of broad-spectrum detection required by this task. Though typically only partially selective, by operating metal oxide sensors with rapid temperature programs that sample many possible interactions between film and analyte, we demonstrated that

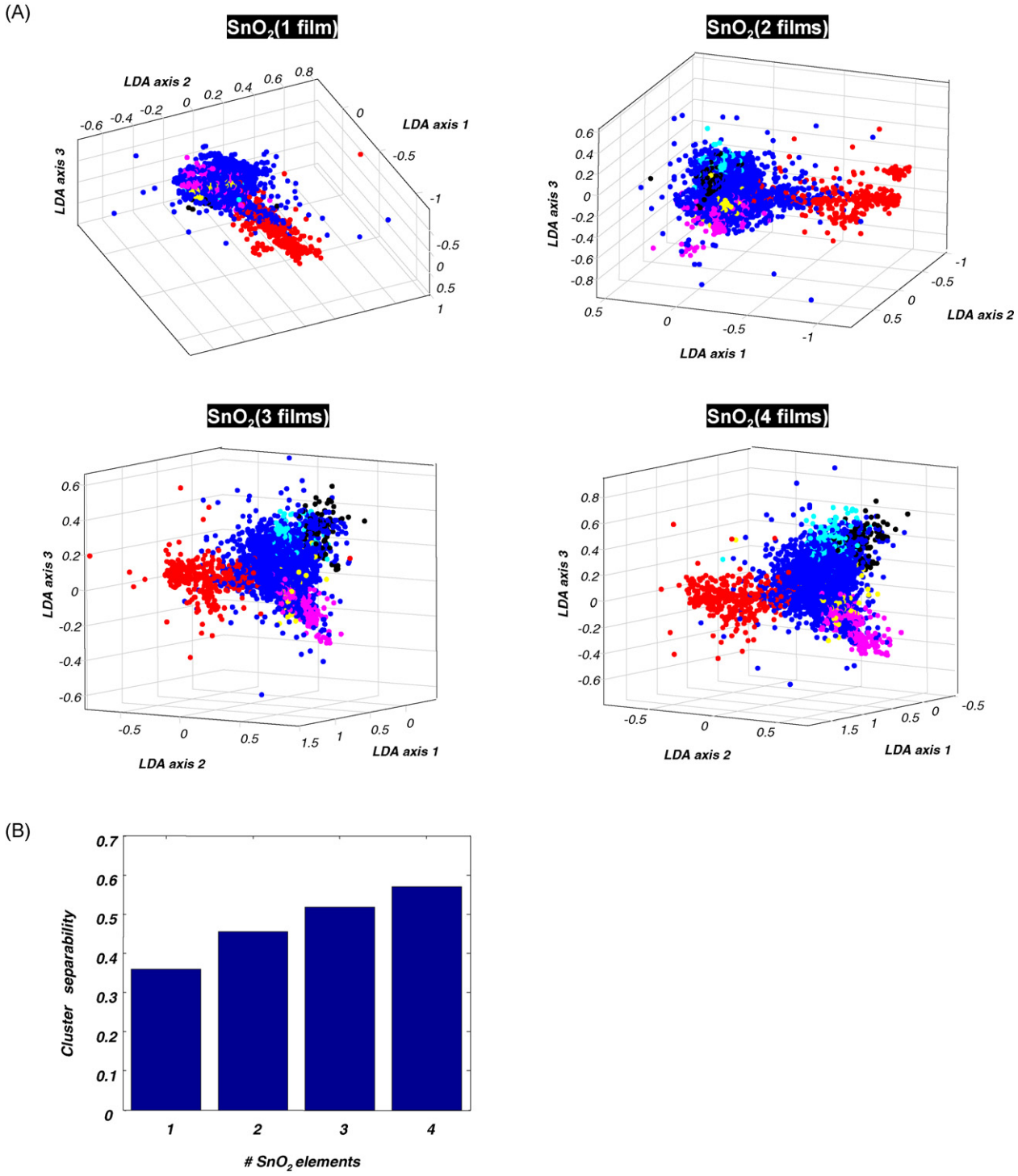

Fig. 13. Benefits of incorporating redundancy into the sensor array. (A) LDA scatter plots as responses from multiple copies of SnO_2 are systematically combined for LDA analysis of five TICs. (B) Quantitative comparison of cluster separability as redundancy is increased.

distinguishable response signatures can be generated for recognition of each of the five TICs.

The selected metal oxide films employed in this study were chosen for two reasons—ease of fabrication and established orthogonal chemical properties. The first, tin oxide (SnO_2), is a widely used transduction material in thick-film sensors [31], and has also been successfully employed in microhotplate arrays [32]. It provides sensitive detection responses for most hydrocarbons. Titanium oxide (TiO_2), while significantly more resistive than SnO_2, exhibits a larger signal range for water vapor [33]. Furthermore, the oxides of titanium and tin have different suboxide states available to them, providing for the possibility of different reaction pathways for incident analytes. It follows that these materials would be expected to produce different conductance signatures for different analytes. The results of this work bear out that conjecture. The hypothesis driving the choice of including SnO_2 and RuO_x into TiO_2 films is as follows: the introduction of electron-rich conducting metal oxides into the lattice of an electron-poor semiconducting metal

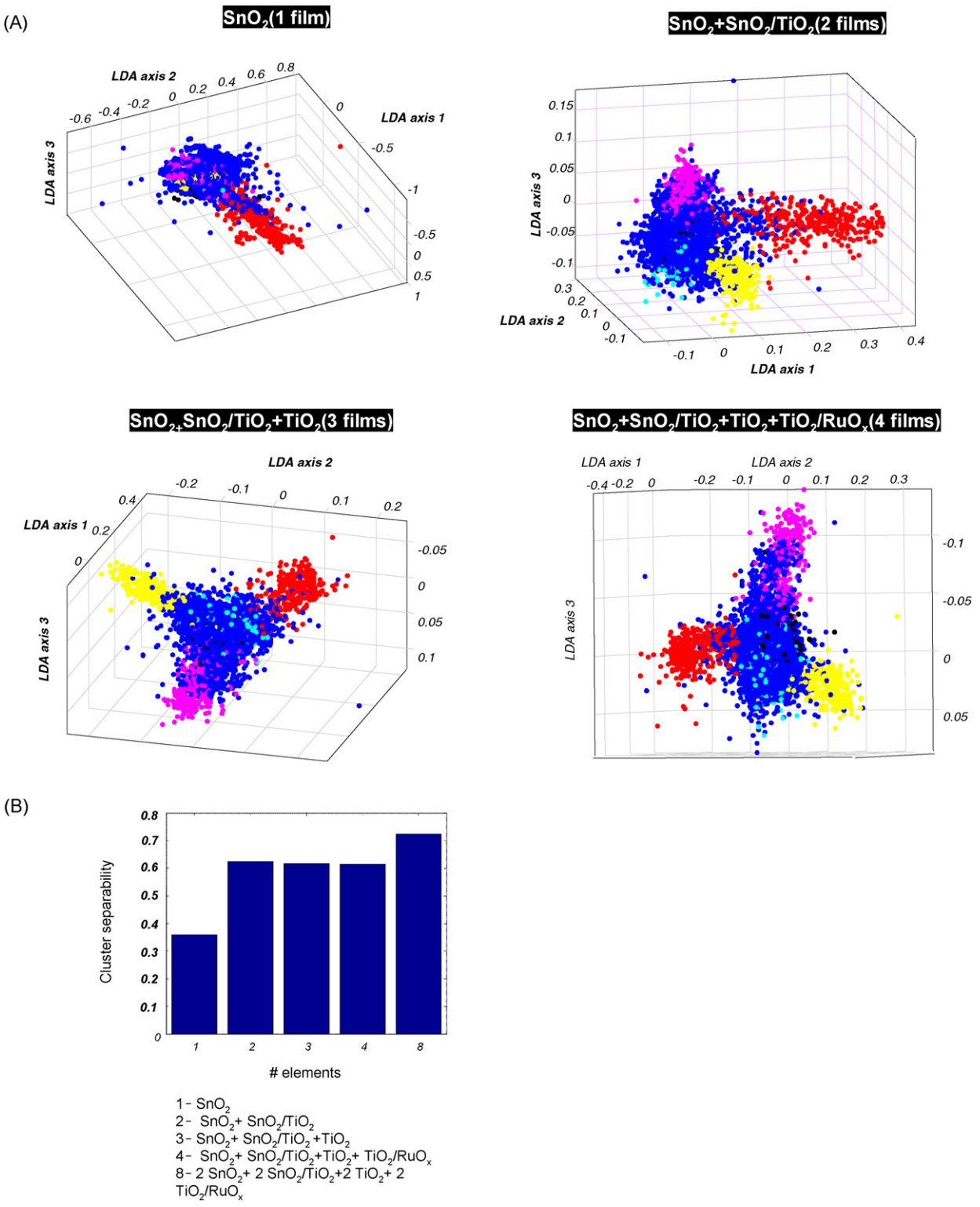

Fig. 14. Benefits of incorporating diversity into the sensor array. (A) Scatter plots as responses from different sensing materials are sequentially added for the analysis of five TICs. (B) Quantitative comparison of cluster separability as different materials are added and multiple copies of each film are used.

oxide is expected to increase the film baseline conductance and concomitantly modify the surface chemistry. The correlation and dimensionality reduction analysis results also support this hypothesis.

We observed that cycling each sensing film through the 32 temperatures shown in Fig. 4 did not necessarily create information that spanned 32 different dimensions. The responses were highly correlated and information seemed to be grouped based on temperature ranges; all lower temperature responses of a film type provide similar information that differs from that available from high temperature signals (see Fig. 6). This is not surprising, as the chemical interactions between analyte and substrate in the operating temperature range are limited largely to adsorption processes (which are expected to dominate at low temperatures) and oxi-

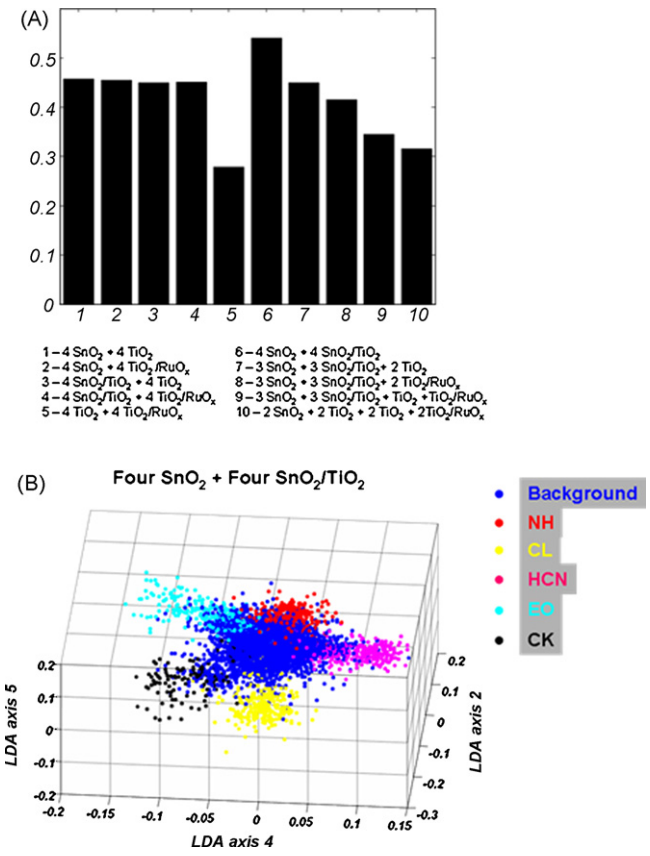

Fig. 15. Optimization of array composition. (A) Comparison of different 8-element array configurations for the problem of recognition of multiple chemical hazards. The objective function is the same as the previous problem, except in this case, all compared solutions have eight array elements ($\gamma_1 = 1$, $\gamma_2 = 0.1$, $\gamma_3 = 0$). The optimal array design in this case is an 8-element array with four elements each of SnO_2 and SnO_2/TiO_2. (B) LDA scatter plot for the best sensor array configuration showing enough analytical information for detecting and identifying each of the five TICs in different background conditions.

dation or decomposition of adsorbed species (which is expected to be kinetically favorable at high temperatures). On the other hand, cross-correlations computed across materials were comparatively lower than self-correlations. Taken together with the results from the dimensionality reduction analysis, this suggests that different materials provide orthogonal information about the target analytes.

Our information content analysis showed that a continuum exists between the TIC clusters and the background cluster. The transient responses immediately before and after introduction and removal of the analytes were not manually removed and spanned the region between the TIC's and the background clusters. For gases like CK and EO, which were slow to evoke response from the sensor array, the transient response phases at the analyte onset and offset were relatively longer and hence resulted in a more prominent continuum. Furthermore, we note again that some analyte presentations were purposefully introduced such that the concentration gradually increased in fixed steps until it reached the IDLH concentration and was likewise removed in a similar gradual fashion. The low concentration measurements during such graded introductions, similar to the transient response measurements, were also distributed in the region between the TIC clusters and the background cluster. These experimental details clearly illustrate the complexity of the chosen problem.

Our study here presents a valuable approach for designing sensor arrays for recognizing chemical hazards. Achieving real-time recognition capabilities and extended operation on the order of weeks to months, however, would involve overcoming additional hurdles imposed by response drift as well as analytical challenges in dealing with unknown targets and backgrounds. We consider these problems elsewhere and present solutions based on related but different approaches to these issues [34,35].

5. Conclusions

To summarize, we have tuned a microsensor array for the problem of identifying certain TICs in the presence of interferences at fixed mixing-ratios and ambient condition changes by controlling the sensor material composition within the array and designing rapid temperature programs that enhance the analytical information obtained from each element in the array as a function of time. We have demonstrated sufficiency of the chosen materials and the temperature program to perform this task. The statistical methods developed, during the course of this work, provide a generalizable methodology for designing and evaluating such array-based solutions for a wide variety of specific detection problems. These advances are critical to the production of pre-programmed microsensors for non-invasive, real-time, multi-species recognition relevant to homeland security and other applications involving trace analyte detection in complex chemical cocktails.

Acknowledgements

We acknowledge partial financial support of this project by the U.S. Department of Homeland Security, Science and Technology Directorate. BR was supported by a NIH(NIBIB)-NIST Joint Postdoctoral Associateship Award administered through the National Research Council. We thank Kurt Benkstein, Mike Carrier, Steve Fick, Jim Melvin, Wyatt Miller, Chip Montgomery, Casey Mungle, Jim Yost, Blaine Young, and Li Zhang for their valuable contributions to this project. We are grateful to Mark Stopfer for helpful comments on an earlier version of this manuscript.

References

[1] G.A. Eiceman, J. Gardea-Torresday, E. Overton, A. Bhushan, H.P. Dharmasena, Gas chromatography, Analytical Chemistry 78 (2006) 3985–3996.
[2] W.A. Bryden, R.C. Benson, H.W. Ko, M. Donlon, Universal agent sensor for counterproliferation applications, Johns Hopkins Apl Technical Digest 18 (1997) 302–308.
[3] G.A. Eiceman, J.A. Stone, Ion mobility spectrometers in national defense, Analytical Chemistry 76 (2004) 390A–397A.
[4] C.E. Kientz, Chromatography and mass spectrometry of chemical warfare agents, toxin and related compounds: state of the art and future prospects, Journal of Chromatography A 814 (1998) 1–23.
[5] D.C. Collins, M.L. Lee, Developments in ion mobility spectrometry-mass spectrometry, Analytical and Bioanalytical Chemistry 372 (2002) 66–73.
[6] W.E. Steiner, S.J. Klopsch, W.A. English, B.H. Clowers, H.H. Hill, Detection of a chemical warfare agent stimulant in various aerosol matrixes by ion mobility time-of-flight mass spectrometry, Analytical Chemistry 77 (2005) 4792–4799.
[7] C.M. Harris, Seeing SAW potential, Analytical Chemistry 75 (2003) 355A–358A.
[8] J.W. Grate, S.L. Rose-Pehrsson, D.L. Venezky, M. Klusty, H. Wohltjen, Smart sensor system for trace organophosphorous vapor detection employing a temperature-controlled array of surface-acoustic-wave sensors, automated preconcentration, and pattern-recognition, Analytical Chemistry 65 (1993) 1868–1881.
[9] S.W. Zhang, T.W. Swager, Fluorescent detection of chemical warfare agents: functional group specific ratiometric chemosensors, Journal of the American Chemical Society 125 (2003) 3420–3421.
[10] S. Bencic-Nagale, T. Sternfeld, D.R. Walt, Microbead chemical switches: an approach to detection of reactive organophosphate chemical warfare agent vapors, Journal of the American Chemical Society 128 (2006) 5401–5408.
[11] M.H. Hammond, K.J. Johnson, S.L. Rose-Pehrsson, J. Ziegler, H. Walker, K. Caudy, D. Gary, D. Tillet, A novel chemical detector using cermet sensors and pattern

recognition methods for toxic industrial chemicals, Sensors and Actuators B 116 (2006) 135–144.
[12] G. Liu, Y. Lin, Electrochemical sensor for organophosphates pesticides and nerve agents using zirconia nanoparticles as selective sorbents, Analytical Chemistry 77 (2005) 5894–5901.
[13] A.A. Tomchenko, G.P. Harmer, B.T. Marquis, Detection of chemical warfare agents using nanostructured metal-oxide sensors, Sensors and Actuators B 108 (2005) 41–55.
[14] A.R. Hopkins, N.S. Lewis, Detection and classification characteristics of arrays of carbon black/organic polymer composite chemiresistive vapor detectors for the nerve agent simulants dimethylphosphonate and diisopropylmethylphosponate, Analytical Chemistry 73 (2001) 884–892.
[15] D.C. Meier, C.J. Taylor, R.E. Cavicchi, E. White, S. Semancik, M.W. Ellzy, K.B. Sumpter, Chemical warfare agent detection using MEMS-compatible microsensor arrays, IEEE Sensors Journal 5 (2005) 712–725.
[16] CHEMWATCH, in http://nist.chemwatch.us/: NIST.
[17] NIOSH, NIOSH Pocket Guide to Chemical Hazards, in http://www.cdc.gov/niosh/npg/default.html: NIOSH Publication No. 2005-149.
[18] Mention of these and any other commercial products is strictly for provision of proper experimental definition, and does not constitute an endorsement by the National Institute of Standards and Technology.
[19] S. Semancik, R.E. Cavicchi, M.C. Wheeler, J.E. Tiffany, G.E. Poirier, R.M. Walton, J.S. Suehle, B. Panchapakesan, D.L. Devoe, Microhotplate platforms for chemical sensor research, Sensors and Actuators B 77 (2001) 579–591.
[20] S. Semancik, R. Cavicchi, Kinetically controlled chemical sensing using micromachined structures, Accounts of Chemical Research 31 (1998) 279–287.
[21] M. Batzill, U. Diebold, The surface and materials science of tin oxide, Sensors and Actuators B 43 (1997) 45–51.
[22] K.J. Albert, N. Lewis, C. Schauer, G.A. Sotzing, S.E. Stitzel, T.P. Vaid, D.R. Walt, Cross-reactive chemical sensor arrays, Chemical Reviews 100 (2000) 2595–2626.
[23] N. Bârsan, U. Weimar, Understanding the fundamental principles of metal oxide based gas sensors; the example of CO sensing with SnO_2 sensors in the presence of humidity, Journal of Physical Condensed Matter 15 (2003) R813–R819.
[24] J. Ding, T.J. McAvoy, R.E. Cavicchi, S. Semancik, Surface state trapping models for SnO_2-based microhotplate sensors, Sensors and Actuators B 77 (2001) 597–613.
[25] G. Gaggiotti, A. Galdikas, S. Kačiulis, G. Mattogno, A. Šetkus, Temperature dependencies of sensitivity and surface chemical composition of SnO_x gas sensors, Sensors and Actuators B 24/25 (1995) 516–519.
[26] CRC Handbook of Chemistry and Physics, 66th ed., in: R.C. Weast (Ed.), CRC, Florida, 1985–1986.
[27] R.O. Duda, P.E. Hart, D.G. Stork, Pattern Classification, 2nd ed., Wiley-Interscience, New York, 2000.
[28] T.C. Pearce, P. Verschure, J. White, J. Kauer, Robust Stimulus Encoding in Olfactory Processing: Hyperacuity and Signal Transmission, vol. 2036, Springer, 2001.
[29] A. Matzger, C.E. Lawrence, R.H. Grubbs, N.S. Lewis, Combinatorial approaches to the synthesis of vapor detector arrays for use in an electronic nose, Journal of Combinatorial Chemistry 2 (2000) 301–304.
[30] S. Bencic-Nagale, D.R. Walt, Extending the longevity of fluorescence-based sensor arrays using adaptive exposure, Analytical Chemistry 77 (2005) 6155–6162.
[31] N. White, J. Turner, Thick-film sensors: past, present and future, Measurement Science and Technology 8 (1997) 1–20.
[32] B. Panchapekesan, R. Cavicchi, S. Semancik, D.L. DeVoe, Sensitivity, selectivity and stability of tin oxide nanostructures on large area arrays of microhotplates, Nanotechnology 17 (2006) 415–425.
[33] D.C. Meier, S. Semancik, Effects of materials chemistry on conductometric sensor signals, in: 2005 Materials Research Society Meeting, Boston, 2005.
[34] B. Raman, J. Hertz, K. Benkstein, S. Semancik, A bioinspired methodology for artificial olfaction, Analytical Chemistry 80 (2008) 8364–8371.
[35] B. Raman, D. Meier, J. Evju, S. Semancik, Towards real-time recognition of a chemical hazard in complex environments with temperature-programmed microsensors, in preparation.

Biographies

Baranidharan Raman received his Bachelor of Engineering in Computer Science with distinction from the University of Madras in 2000, and the MS and Ph.D. degrees in Computer Science from Texas A&M University in 2003 and 2005, respectively. He is currently a joint NIH/NIST postdoctoral fellow working in the Laboratory of Cellular and Synaptic Neurophysiology (NIH) on biological olfaction, and in the Process Sensing Group (NIST) on artificial olfaction. His research interests include combining computational and electrophysiological approaches to study neural computations, sensor-based machine olfaction, intelligent systems, machine learning and dynamical systems.

Douglas C. Meier holds a B.A. in Chemistry from Northwestern University and a Ph.D. in Chemistry from Texas A&M University, where he studied the chemical physics of model catalyst systems under the guidance of Professor D. Wayne Goodman. Dr. Meier was subsequently awarded a National Research Council Postdoctoral Research Associateship in the Process Sensing Group at the National Institute of Standards and Technology (NIST), during which he applied his training in surface chemistry and thin film science to the development of advanced chemical microsensor arrays. For these efforts, he was awarded the United States Department of Commerce Silver Medal. Currently a NIST Research Chemist in the Surface and Microanalysis Science Division, Dr. Meier utilizes tools such as Auger Electron Microscopy to perform fundamental studies on materials at the nanoscale.

Jon K. Evju was born in Oslo, Norway in 1967 and is a Research Chemist working in the Solid State Chemical Microsensor Program at the National Institute of Standards and Technology (NIST). After completing high school at Hartvig Nissen VGS in Oslo, he attended University of Wisconsin at River Falls and received his BS in Chemistry in 1992. He was awarded a Ph.D. in Chemistry from University of Minnesota, Minneapolis in 2000, for his graduate work on organometallic compounds, performed under direction of Professor Kent R. Mann. Upon completion of his thesis research, he joined Professor W.H. (Bill) Smyrl's research group at University of Minnesota, Department of CEMS as a Postdoctoral Research Associate and led the *f*-NSOM project to improve the technique and achieve <50 nm lateral resolution in scanning electrochemical microscopy. He joined NIST as a Guest Researcher in 2001 and worked to develop surface modification techniques for microfluidic polymer devices. In 2003, he was hired by NIST and has since earned recognition and awards within NIST and the Department of Commerce for performing realistic gas sensing experiments and for scientific merits associated with lowering limits of detection for the microhotplate gas sensors.

Steve Semancik is the Project Leader of the Chemical Microsensor Program at the National Institute of Standards and Technology (NIST) in Gaithersburg, Maryland. He received his B.S. degree in physics from Rensselaer Polytechnic Institute and his Sc.M. and Ph.D. degrees, also in physics, from Brown University. Dr. Semancik's professional research career began as a National Research Council Postdoctoral Fellow, and has been centered in the fields of surface science and sensor science. His recent work has focused on developing improved nanomaterials for chemical and biochemical sensing, and combining such high performance materials with micromachined platforms to realize advanced microsensor devices and operating modes. He has authored or coauthored 132 papers (including five reviews), one book chapter, and five patents. Dr. Semancik is an elected Fellow of both the American Physical Society and the American Vacuum Society, has served as a Member of the Editorial Board of two sensor journals, and is a Member of the Steering Committee of the International Meeting on Chemical Sensors.